Critical pore radius and transport properties of disordered hard- and overlapping-sphere models

Michael A. Klatt [1,2,*] Robert M. Ziff [3,†] and Salvatore Torquato [1,4,‡]

[1]*Department of Physics, Princeton University, Princeton, New Jersey 08544, USA*

[2]*Institut für Theoretische Physik, FAU Erlangen-Nürnberg, Staudtstr. 7, 91058 Erlangen, Germany*

[3]*Center for the Study of Complex Systems and Department of Chemical Engineering, University of Michigan, Ann Arbor, Michigan 48109, USA*

[4]*Department of Chemistry, Princeton Institute for the Science and Technology of Materials, and Program in Applied and Computational Mathematics, Princeton University, Princeton, New Jersey 08544, USA*

(Received 20 April 2021; accepted 29 June 2021; published 22 July 2021)

Transport properties of porous media are intimately linked to their pore-space microstructures. We quantify geometrical and topological descriptors of the pore space of certain disordered and ordered distributions of spheres, including pore-size functions and the critical pore radius δ_c. We focus on models of porous media derived from maximally random jammed sphere packings, overlapping spheres, equilibrium hard spheres, quantizer sphere packings, and crystalline sphere packings. For precise estimates of the percolation thresholds, we use a strict relation of the void percolation around sphere configurations to weighted bond percolation on the corresponding Voronoi networks. We use the Newman-Ziff algorithm to determine the percolation threshold using universal properties of the cluster size distribution. The critical pore radius δ_c is often used as the key characteristic length scale that determines the fluid permeability k. A recent study [Torquato, Adv. Wat. Resour. **140**, 103565 (2020)] suggested for porous media with a well-connected pore space an alternative estimate of k based on the second moment of the pore size $\langle\delta^2\rangle$, which is easier to determine than δ_c. Here, we compare δ_c to the second moment of the pore size $\langle\delta^2\rangle$, and indeed confirm that, for all porosities and all models considered, δ_c^2 is to a good approximation proportional to $\langle\delta^2\rangle$. However, unlike $\langle\delta^2\rangle$, the permeability estimate based on δ_c^2 does not predict the correct ranking of k for our models. Thus, we confirm $\langle\delta^2\rangle$ to be a promising candidate for convenient and reliable estimates of the fluid permeability for porous media with a well-connected pore space. Moreover, we compare the fluid permeability of our models with varying degrees of order, as measured by the τ order metric. We find that (effectively) hyperuniform models tend to have lower values of k than their nonhyperuniform counterparts. Our findings could facilitate the design of porous media with desirable transport properties via targeted pore statistics.

DOI: 10.1103/PhysRevE.104.014127

I. INTRODUCTION

The statistics that structurally or topologically characterize the pore space of disordered porous media are intimately linked to their effective transport properties, such as the effective electrical conductivity σ_e [1], mean survival time $\overline{T}$ [2–4], principal (largest) diffusion relaxation time T_1 [2,3], and principal viscous relaxation time Θ_1 [5]. For example, the first and second moments of the pore-size probability density function $P(\delta)$, $\langle\delta\rangle$ and $\langle\delta^2\rangle$, respectively, bound $\overline{T}$ and T_1 from above for diffusion-controlled reactions in which the interface of the porous medium is perfectly absorbing for a solute species diffusing in the pore space, where $P(\delta)d\delta$ is the probability that a randomly chosen point in the pore space lies at a distance between δ and $\delta + d\delta$ from the nearest point on the pore-solid interface [1].

An especially important pore characteristic is the *critical pore radius* δ_c of a heterogeneous material, which is the maximal radius of an impenetrable test sphere so that the sphere can percolate through the void space. Interestingly, as detailed below, the critical pore radius δ_c is related not only to all of the aforementioned effective transport properties $(\sigma_e, \overline{T}, T_1, \Theta_1)$ of the porous medium but also to its fluid permeability.

The *fluid permeability* k associated with slow viscous flow through an isotropic porous medium is defined by Darcy's law, which can be rigorously derived using homogenization theory [6]. The permeability k has dimensions of the square of length and, roughly speaking, may be regarded as an effective pore channel area of the dynamically connected part of the pore space [1]. Avellaneda and Torquato [5] used the solutions of unsteady Stokes equations for the fluid velocity vector field to derive a general rigorous relation connecting the fluid permeability k to the formation factor $\mathcal{F}$ of the porous medium and a length scale $\mathcal{L}$ that is determined by the eigenvalues of the Stokes operator:

$$k = \frac{\mathcal{L}^2}{\mathcal{F}}, \tag{1}$$

*mklatt@princeton.edu
†rziff@umich.edu
‡torquato@princeton.edu

where $\mathcal{L}$ is a certain weighted sum over the *viscous relaxation times* Θ_n (i.e., inversely proportional to the eigenvalues of the Stokes operator), and $\mathcal{F} = \sigma_1/\sigma_e$ is the formation factor, where σ_e is the effective electrical conductivity of a porous medium with a conducting fluid of conductivity σ_1 and a solid phase that is perfectly insulating. Roughly speaking, the formation factor $\mathcal{F}$ quantifies the degree of windiness for electrical transport pathways across a macroscopic sample [7]. (Note that the length scale $\mathcal{L}$ appearing in (1) absorbs a factor of 8 compared to the definition L given in Ref. [5]; specifically, $\mathcal{L} = L/8$.)

The prediction of the fluid permeability via theoretical methods is a notoriously difficult problem, largely because it is nontrivial to estimate the length scale $\mathcal{L}$ in (1) for general porous media. Thus, the majority of previous analytical studies attempt to provide closed-form estimates of $\mathcal{L}$. For example, the length scale $\mathcal{L}$ can be rigorously bounded from above by length scales associated with the mean survival time $\overline{T}$ [8], principal diffusion relaxation time T_1 [3], and principal viscous relaxation time Θ_1 [5]. There is a panoply of approximation formulas for $\mathcal{L}$ [1,9–11]. An estimate due to Katz and Thompson [10] approximates $\mathcal{L}$ to be proportional to the capillary radius at breakthrough during mercury injection in the pore space, which is directly related to the critical pore radius δ_c [12]. Empirical correlations between permeability and critical pore radius have also been found using the water expulsion method [13].

The critical pore radius is a complex structural characteristic that encodes both nontrivial geometrical and topological information. Motivated by rigorous bounds on the principle relaxation time T_1 and its link to the permeability, Torquato [7] suggested the second moment of the pore size $\langle\delta^2\rangle$ as an easily measurable approximation of $\mathcal{L}^2$ for models where the pore space is well connected. The approximation was verified for BCC sphere packings [7]. Thus, $\langle\delta^2\rangle$ is expected to be closely related to the critical pore radius, which we verify below.

Here, we study the critical pore radius and void percolation for disordered and ordered models of porous media derived from either overlapping or hard spheres (HS) with a constant radius R. Such configurations of overlapping or hard spheres are effective models of a broad range of heterogeneous materials and many-particle systems [1,14–18]. Our models exhibit a varying degree of long- and short-range order, from completely random overlapping spheres to the crystalline densest packing of hard spheres.

Importantly, we determine the critical pore radius of maximally random jammed (MRJ) packings of identical spheres [19], which are, intuitively speaking, the maximally disordered among all mechanically stable packings. More precisely, MRJ sphere packings minimize among jammed packings an order metric Ψ [19–26]. Previously studied structural characteristics of MRJ sphere packings include their two-point statistics, average contact numbers, fractions of rattlers, Voronoi cell statistics and correlation functions, pore-size distributions, etc. [20,27–30]. Bounds on transport properties of MRJ packings have been recently characterized in Ref. [31]. Ziff and Torquato [32] determined the site and bond percolation threshold of MRJ sphere packings.

We compare the critical pore radius of the MRJ sphere packings to three crystalline sphere packings and to three models with disordered microstructures. The first model is that of overlapping spheres that are completely random and independent (also known as the Swiss-cheese model) [1], and the second model is that of equilibrium hard spheres [18]. For the third model, we assign overlapping spheres to the points of amorphous inherent structures of the quantizer energy [33], where the quantizer energy is proportional to the first moment of the void exclusion probability $E_V(r)$ (which is the probability that a randomly placed spherical cavity of radius r contains no points) [34]. Hence, the quantizer energy is also related to the pore-size distribution [31]. We therefore suggest it as an interesting model for studying transport properties. For both the overlapping spheres (or Swiss-cheese model) and the quantizer model, we consider two different diameters of the spheres: (i) the average nearest-neighbor distance and (ii) diameters that result in the same porosity as MRJ sphere packings.

We quantify the degree of short-, intermediate-, and long-range order in our four systems using the τ order metric [35]. It measures how the two-point statistics deviate from those of the Poisson point process:

$$\begin{aligned}\tau &:= \frac{1}{D^d}\int_{\mathbb{R}^d}[g_2(\boldsymbol{r})-1]^2 d\boldsymbol{r}\\ &= \frac{1}{(2\pi)^d D^d \rho^2}\int_{\mathbb{R}^d}[S(\boldsymbol{k})-1]^2 d\boldsymbol{k},\end{aligned} \tag{2}$$

where $g_2(\boldsymbol{r})$ is the pair-correlation function and $S(\boldsymbol{k})$ the structure factor [1,18]. The systems are compared at unit number density (with a cutoff value $k = 16.5$ for the integration in Fourier space).

Here, we estimate the void percolation threshold using Kerstein's method [36], as described in Sec. II, and the Newman-Ziff algorithm [37]. The latter is based on the second moment of the cluster sizes and allows for a convenient finite-size scaling.

As mentioned above, Torquato [7] recently suggested for porous media with a well-connected pore space to use the second moment of the pore size, $\langle\delta^2\rangle$, as a convenient estimate of $\mathcal{L}^2$, which in turn allows an estimation of the fluid permeability k. Here, we compare the critical pore radius δ_c to $\langle\delta^2\rangle$ and confirm that to a good approximation $\delta_c^2 \propto \langle\delta^2\rangle$. In fact, we find that an estimation of k based on $\langle\delta^2\rangle$ is superior to an estimate based on δ_c in that only the former provides the correct ranking of k for our models.

We also compare the fluid permeability of models with different large-scale density fluctuations, i.e., nonhyperuniform and hyperuniform models. A hyperuniform porous medium is defined by an anomalous suppression of long-wavelength volume-fraction fluctuations compared to those of typical disordered media [38–40]. In agreement with the analysis of Torquato [7], we find that the estimates of fluid permeabilities for our hyperuniform models tend to be smaller than those of their nonhyperuniform counterparts.

In the following, we first define our models, construction of Voronoi networks, and clustering analysis in Sec. II. Then, we present our results on the critical pore radius, the pore statistics, and estimates of the fluid permeability in Sec. III. In Sec. IV, we give concluding remarks and an outlook to future research.

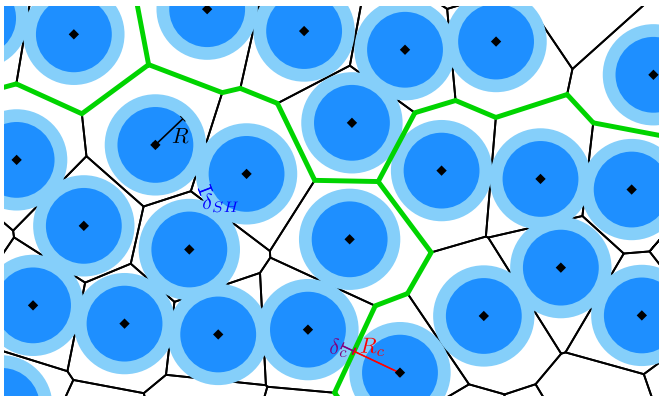

FIG. 1. Two-dimensional schematic of how the critical pore size δ_c of a dispersion of hard disks (dark blue or gray) can be determined from the corresponding Voronoi diagram (black) [36]. Each bond in the Voronoi diagram corresponds to a channel in the void space. When each disk of radius R is surrounded by a soft shell of thickness δ_{SH} (light blue or gray), then δ_c is equal to the critical thickness at which the pore space ceases to percolate; the thick (green) line highlights a cluster of open channels.

II. MODELS AND STRUCTURE CHARACTERIZATION

We use periodic boundary conditions for all of our samples, the construction of the Voronoi network, and the percolation analysis. Figure 1 schematically shows how the pore space is related to the Voronoi network.

Models. The first model is that of overlapping spheres that are randomly and uniformly distributed in the simulation box without interaction. Hence, the sphere centers are a snapshot of the ideal gas in the canonical ensemble, i.e., the number N of points per sample is fixed. Mathematically speaking, the points follow a binomial point process. The τ order metric for this model is 0, by definition.

The second model that we study is an equilibrium fluid of hard spheres. The equal-sized spheres are impenetrable but do not interact otherwise. Each sample has a packing fraction of 45%. The τ order metric is 9.45(1).

Determining the critical pore radius of equilibrium hard spheres is closely related to the so-called *cherry-pit model* [1], where each hard sphere of radius R is surrounded by a penetrable spherical shell of thickness δ_{SH}. The thickness at which the void space (outside the penetrable spheres) stops percolating is the critical pore radius δ_c. It is, therefore, strictly related to the void percolation threshold $R_c := R + \delta_c$. The same principle applies to any other monodisperse sphere configuration; see Fig. 1 for a two-dimensional schematic.

The third model is that of maximally random jammed (MRJ) packings of hard spheres. Here, we analyze packings generated by Atkinson *et al.* [28]. The average packing fraction is 63.6%. The τ order metric is 23.7(1) [33].

The fourth model is based on amorphous inherent structures of the quantizer energy [33]. This energy functional is defined for Voronoi tessellations of arbitrary point configurations [33,34,41–47], and it is proportional to a sum of the second moments of inertia of all Voronoi cells (each computed with respect to the corresponding Voronoi center). The quantizer energy can be interpreted as a many-body interaction with a certain soft-core repulsion [34]. It has been studied both as a ground-state problem [34] and at finite temperature [44–47].

More precisely, the quantizer energy can be defined as the first moment of the void exclusion probability $E_V(r)$ of the point configuration. For a point pattern at unit number density, the rescaled quantizer energy (or error) is given by [34]:

$$\mathcal{G} := \frac{1}{d}\langle r^2\rangle = \frac{2}{d}\int_0^\infty r E_V(r)\,dr, \tag{3}$$

where d is the dimension (here $d = 3$). For monodisperse sphere packings with radius R, the complementary cumulative distribution function $F(\delta)$ of the pore size is trivially related to the exclusion probability via $E_V(r) = \phi_1 F(r - R)$ for $r > R$, where ϕ_1 is the volume fraction of the pore space (and $\phi_2 = 1 - \phi_1$ is the volume fraction of the spheres) [1]. Hence, the quantizer energy is closely related to the second moment of the pore size $\langle\delta^2\rangle = 2\int_0^\infty \delta F(\delta)\,d\delta$; in fact, for point particles with $R = 0$: $\mathcal{G} = \langle\delta^2\rangle/d$; and for nonoverlapping spheres, the following relation can be straightforwardly derived by using Eq. (5.68) in Torquato [1]:

$$\mathcal{G} = \frac{3 + 2\phi_1}{5d}R^2 + \frac{2\phi_1}{d}R\langle\delta\rangle + \frac{\phi_1}{d}\langle\delta^2\rangle. \tag{4}$$

Optimizing the quantizer energy for the centers of a sphere packing is, therefore, closely related to an optimization of its pore statistics.

To construct our samples of amorphous inherent structures, we start from a binomial point process and locally minimize the quantizer energy using the Lloyd algorithm [33]. In each step of the algorithm and for each cell, the Voronoi center is replaced by the center of mass of the cell [49]. We apply 10000 steps, after which the algorithm converges to an amorphous inherent structure with a strong suppression of density fluctuations [33]. The final states are (effectively) centroidal Voronoi tessellations, where in each cell the Voronoi center coincides with the center of mass. The quantizer energy of the disordered inherent structures ($\mathcal{G} = 0.07917$) is only slightly larger than that of the (conjectured) crystalline ground state, the body-centered cubic (BCC) lattice ($\mathcal{G} = 0.07854$) [33]. The τ order metric of the amorphous inherent structures of the quantizer energy is 31.6(2) [33], i.e., larger than the value for MRJ sphere packings by about a factor of 4/3.

The corresponding ground-state problem, known as the quantizer problem, is also related to another tessellation optimization problem, known as the covering problem [34]. The latter problem is the search for a point configuration that minimizes the radius of overlapping circumscribed spheres to cover the space. This covering radius is always an upper bound on the critical radius R_c. Since MRJ sphere packings are saturated, they have a finite covering radius, like a crystal. A finite covering radius $R_{\text{cov}} < \infty$ implies that the exclusion probability $E_V(r)$ has compact support, specifically, $E_V(r) = 0$ for $r \geqslant R_{\text{cov}}$. As for the quantizer problem, the BCC lattice is believed to be the optimum of the covering problem. Both the quantizer and covering problems have relevance in numerous applications, from wireless communication and network layouts, to data compression and cryptography; see Torquato [34] and references therein.

TABLE I. The number of samples and number points per sample for each of our models.

Overlapping spheres	Equilibrium HS
20000 × 1000 points	2000 × 500 points
10000 × 2000 points	1000 × 1000 points
5000 × 4000 points	200 × 5000 points
1000 × 10000 points	100 × 10000 points
MRJ HS	**Quantizer spheres**
	2000 × 500 points
1015 × 2000 points	1000 × 1000 points
	200 × 5000 points
16 × 10000 points	100 × 10000 points

We compare the pore statistics and transport properties of our four disordered models to those of three perfectly ordered crystalline structures. Specifically, we here consider dense lattice packings of spheres with simple cubic (SC), body-centered cubic (BCC), and face-centered cubic (FCC) symmetries.

Simulation details. The MRJ samples are simulated in unit cells with a nonorthogonal basis. All other samples are simulated in cubic unit cells. Table I lists the number of samples and the number of points per sample. The total number of points in our samples is more than 80×10^6. The number density ρ is the average number of points per unit volume. We choose the unit of the length such that $\rho = 1$ for all of our models. For the overlapping and equilibrium hard spheres and for the quantizer sphere configurations, the number density is fixed for each sample. For the MRJ spheres packings, the radius of the spheres is fixed, but the number density slightly fluctuates around unity. Figures 2–6 show for each of our models a sample of the void space.

Voronoi network. For monodisperse sphere configurations, the void percolation can be accurately studied by reformulating it as a weighted bond percolation on the Voronoi network, as discussed by Kerstein [36]; see Fig. 1. The topology of the void space is related to that of the Voronoi network, i.e., the network formed by the edges of the Voronoi diagram. Each channel in the void space corresponds to a bond in the Voronoi network. The channel vanishes when $R + \delta_{SH}$ is larger or equal to the distance of the bond to its Voronoi neighbors. Kerstein's method [36] has been previously used to study void percolation for overlapping spheres [48,50–52] and hard-sphere packings (both jammed and in equilibrium) [53], including models for protein structures [54].

Following this idea by Kerstein [36], we construct for each sample the Voronoi diagram using VORO++ [55,56]. By identifying vertices within an accuracy of about 10^{-12}, we determine the Voronoi network (of cell edges) and assign to each edge the smallest distance to its neighboring Voronoi centers. The void percolation problem is thus equivalent to a weighted bond percolation problem on the Voronoi network.

Newman-Ziff method. Our goal was to find the critical percolation threshold of the void system. Along each bond in the Voronoi network, we assigned a weight equal to the distance of the bond to the neighboring Voronoi centers (which is directly related to the radius of a sphere that can just pass through that pore throat), and the goal is to find the critical radius of a sphere where the system percolates. Various criteria can be used to determine the percolation point. A common one has been the point where a single cluster of connected vertices spans from one side of the system to the other, or for a periodic system, where it wraps around. However, various other criteria can be used, including Binder-type ratios [57] involving moments of the size of the largest cluster. The goal in these is to find something universal so that its value is independent of the size of the system under finite-size scaling (although the corrections to scaling will cause a size dependence visible for smaller systems). Here we use another universal quantity: the second moment of the size distribution

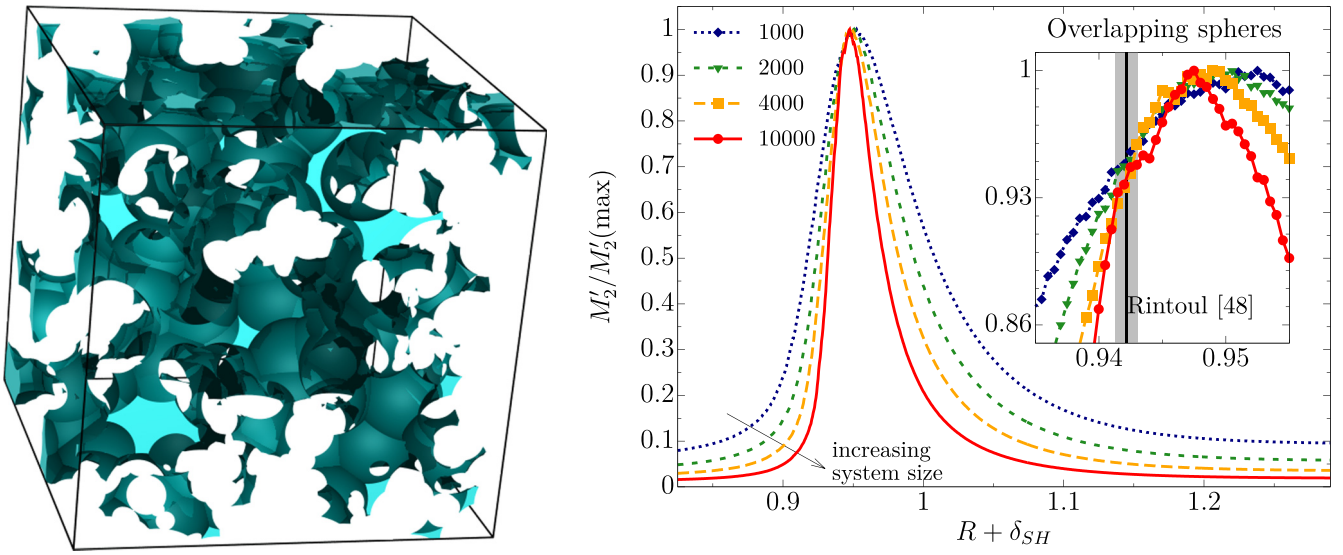

FIG. 2. Overlapping spheres: a sample of the void space (left) and the rescaled cluster index M_2' as a function of the sphere radii $R + \delta_{SH}$. The curves for different system sizes intersect (see inset) roughly in one point, which corresponds to the percolation threshold R_c. The value agrees within statistical accuracy with the previous result by Rintoul [48], where the mean value is indicated by the vertical line and the error by the gray band. In the sample of the void space the different colors (shades) are only for an improved three-dimensional visualization.

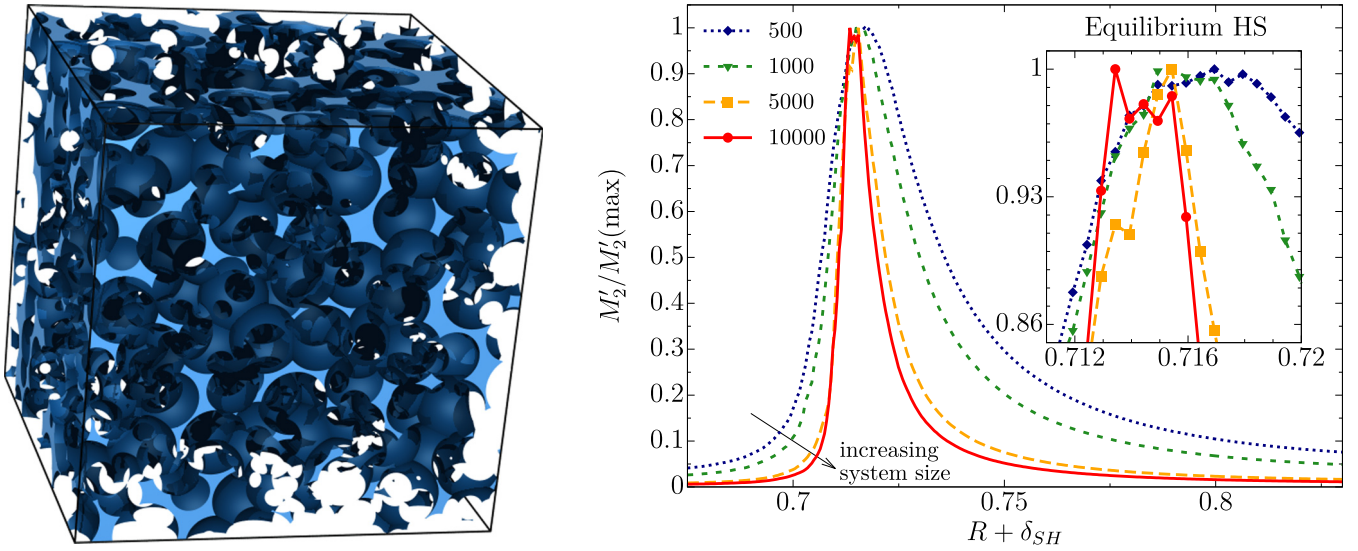

FIG. 3. Equilibrium hard spheres: a sample of the void space surrounding the dilated, cherry-pit spheres with radius $R+\delta_{SH}$ (left) and the rescaled cluster index M_2' as a function of the sphere radii $R+\delta_{SH}$; for more details, see Fig. 2.

leaving out the largest cluster, M_2', divided by its value at the maximum of the curve $M_2'(\max)$. The idea behind this is that M_2' is a peaked function whose peak is near the percolation threshold p_c but not exactly at p_c. Finite-size scaling theory implies that $L^{-\gamma/\nu}M_2'(p)$ becomes a function of $(p-p_c)L^{1/\nu}$ in the scaling limits $p\to p_c$ and $L\to\infty$. If we divide the value at p_c by the value at the maximum, for example, then we get a ratio, which is universal (the same for all systems of the same dimensionality and shape). Thus, if we consider plots of $M_2'(p)/M_2'(\max)$, the crossing of the curves will indicate the critical point. For very precise determinations of the critical point, one would also have to worry about the corrections-to-scaling contribution, but to the precision available for the systems here, this is not necessary.

In the Newman-Ziff algorithm, bonds are added one at a time, and the union-find computer science algorithm is used to keep track of the evolving cluster size distribution in a very efficient manner, including the moments such as M_2'. This is, in fact, much easier than determining crossing or wrapping, which requires extra components in the data structure. Before carrying out the algorithm, we sort all the bonds from large to small weights and then add the bonds one at a time (largest weights first). Thus, for a given sample of a lattice, we could only carry out one test of the percolation threshold, unlike in typical lattices where we could create many measurements by occupying the bonds in random order. Here the order of the bonds is fixed by their weight. The algorithm works in a microcanonical space where averaged quantities are determined as a function of the number of bonds made occupied. Usually, one carries out a convolution of the microcanonical measurements with a binomial distribution to get the canonical behavior that gives results as a function of

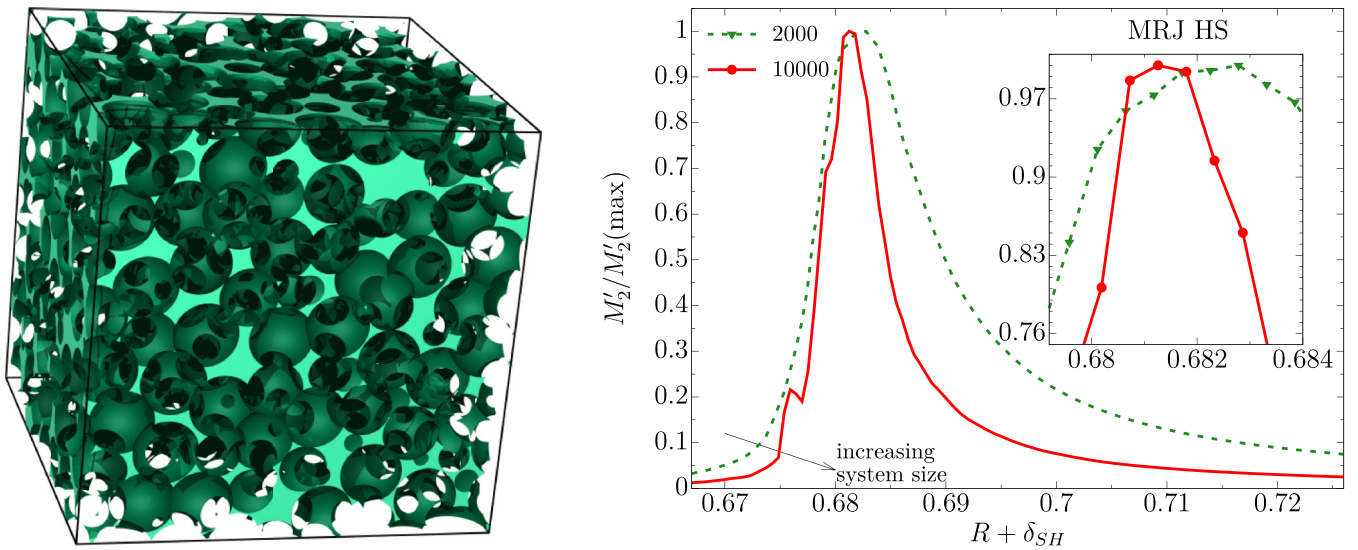

FIG. 4. MRJ hard spheres: a sample of the void space surrounding the dilated, cherry-pit spheres with radius $R+\delta_{SH}$ (left) and the rescaled cluster index M_2' as a function of the sphere radii $R+\delta_{SH}$; for more details, see Fig. 2.

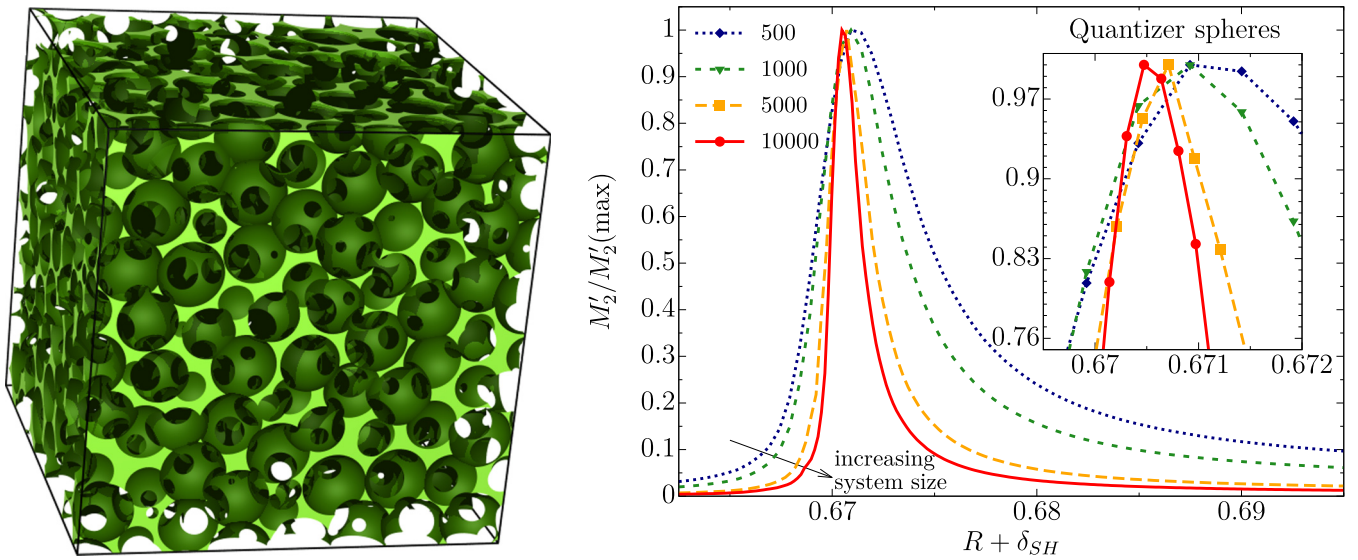

FIG. 5. Quantizer spheres: a sample of the void space surrounding the dilated, cherry-pit spheres with radius $R + \delta_{SH}$ (left) and the rescaled cluster index M_2' as a function of the sphere radii $R + \delta_{SH}$; for more details, see Fig. 2.

p. Here we do not do that, because for one thing there is no random bond occupation probability p here, and, secondly, the difference between the two is slight and would not be observable with the precision of the results that we are able to get here. Since M_2' can strongly fluctuate between samples, we first bin, for each model and system size separately, all weights that we find (using a constant bin width). Then, we average the corresponding values of M_2' within each bin.

The crossing point of $M_2'/M_2'(\max)$ is used to find the threshold. Its value should be universal and the same for all systems of the same shape and boundary conditions. We verified this by considering bond percolation on the simple cubic lattice, and confirm the threshold of $p_c = 0.24881$ with a crossing point of $M_2'/M_2'(\max) = 0.96$, consistent with the values found here (about 0.94–0.96) for these quite different systems.

Pore size. The pore size δ can be easily estimated from both simulated data and three-dimensional images of real porous media [58]. Here, we determine the mean pore size $\langle\delta\rangle$ and the second moment of the pore size $\langle\delta^2\rangle$ using a straightforward Monte Carlo sampling. Points are placed randomly and uniformly distributed in the pore space surrounding the spheres. For each point, we determine the smallest distance to a sphere and estimate the first and second moment of δ using the arithmetic mean. We estimate the statistical error using the standard error of the mean. The number of Monte Carlo points per sample is 10^5, where for each model we analyze each sample of the two largest system sizes. For overlapping spheres, the pore-size distribution is known analytically. We also determine the pore sizes for lattice packings of spheres, where we use 10^7 sampling points for each lattice. For the tabulated values of $\langle\delta\rangle$ and $\langle\delta^2\rangle$ of the dense hard-sphere lattice packings, we use the values from Eqs. (B24)–(B39) in Ref. [31], which were obtained by numerical integration of exact formulas [59]. For the SC and BCC sphere packings, we also confirm these values by numerical integration of the exact formulas for $E_V(R)$ from Eqs. (84) and (87) in Ref. [34]. An exact formula of $E_V(R)$ also allows for precise values of the critical void porosity $\varphi_c := E_V(R_c)$ of the void space surrounding the soft shells at the critical radius.

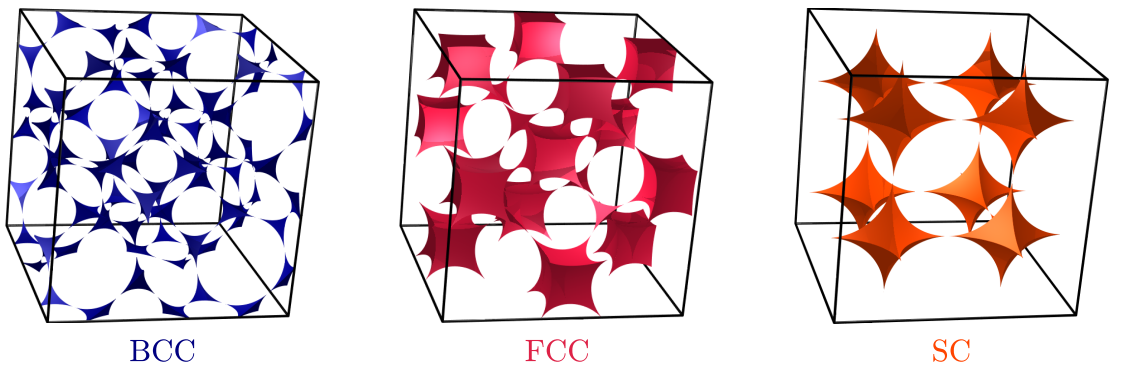

FIG. 6. Void space surrounding the soft overlapping shells at the critical point for BCC (left), FCC (center), and SC (right) crystalline sphere configurations: The different colors (shades) are only for an improved three-dimensional visualization. The critical porosity $\varphi_c := E_V(R_c)$ is distinctly smaller for the BCC spheres than for the FCC and SC spheres.

TABLE II. Void percolation and pore-size statistics for our models with different porosities ϕ_1: The table shows the critical radius R_c, the critical void porosity φ_c (surrounding the soft shells at the critical point), and it compares the critical pore radius δ_c to $\langle\delta^2\rangle$. While R_c and φ_c only depend on the positions of the sphere centers, δ_c and $\langle\delta^2\rangle$ also depend on the radius R and hence on the porosity ϕ_1. For the overlapping spheres and the quantizer model, the table shows the values for two different porosities: for a radius that matches half the nearest-neighbor distance and for a porosity that matches the MRJ value.

Model	ϕ_1	R_c	φ_c	δ_c	$\langle\delta^2\rangle$
Overlapping spheres	0.9148...	0.943(3)	0.0298(10)	0.666(3)	$1.274... \times 10^{-1}$
	0.3640...	0.943(3)	0.0298(10)	0.320(3)	$3.321... \times 10^{-2}$
Equilibrium HS	0.550	0.714(2)	0.0257(12)	0.239(2)	$1.5562(5) \times 10^{-2}$
SC HS	0.4764...	0.707...	0.0349...	0.207...	$1.388... \times 10^{-2}$
Quantizer spheres	0.430	0.670(1)	0.0179(8)	0.156(1)	$6.793(2) \times 10^{-3}$
	0.364	0.670(1)	0.0179(8)	0.136(1)	$5.269(2) \times 10^{-3}$
MRJ HS	0.364	0.681(2)	0.0303(16)	0.148(2)	$7.177(2) \times 10^{-3}$
BCC HS	0.3198...	0.668...	0.0055...	0.122...	$3.718... \times 10^{-3}$
FCC HS	0.2595...	0.648...	0.0358(6)	0.086...	$3.592... \times 10^{-3}$

III. RESULTS

Figures 2–5 show for our four models of disordered sphere configurations the curves of the rescaled cluster index M_2' as a function of the sphere radii $R + \delta_{SH}$. The insets zoom into the region where the curves of different system sizes intersect, i.e., at the percolation threshold R_c in the infinite-system size limit (where R_c is the critical value of $R + \delta_{SH}$). Each figure also shows a sample of the void space for radii below the percolation threshold (about 90% of R_c).

Table II lists our estimates of the critical radius R_c, critical void porosity $\varphi_c := E_V(R_c)$, and critical pore radius δ_c. The table compares the values for the disordered sphere configurations to those of the crystalline sphere configurations. Our results for R_c and φ_c of the overlapping sphere model and equilibrium hard spheres agree within statistical errors with previous results [48,50–53,60]. In particular, for the overlapping spheres $R_c = 0.943(3)$ and $\varphi_c = 0.0298(10)$ agree with the estimates $R_c = 0.942(1)$ and $\varphi_c = 0.0301(3)$ by Rintoul [48], $R_c = 0.9425(9)$ and $\varphi_c = 0.0300(3)$ by Höfling *et al.* [51], and $R_c = 0.9422(3)$ and $\varphi_c = 0.0301(1)$ by Priour and McGuigan [52]. Moreover, our estimate $R_c = 0.714(2)$ for the equilibrium hard spheres agrees with the estimate of $R_c = 0.712(4)$ that we obtain from Fig. S1 in Spanner *et al.* [53].

For our disordered sphere models, we find that the percolation threshold R_c decreases with increasing order, as measured by the τ order metric. Moreover, while the amorphous hard-sphere packings have a distinctly larger value of R_c than the optimal FCC packing, the amorphous quantizer states have about the same R_c as the (conjectured) optimal quantizer, a BCC lattice. The values agree within 0.3%. For the corresponding dispersions of spheres, we find for all radii considered here that the second moment of the pore size, $\langle\delta^2\rangle$ agrees within 0.2% (even if the spheres overlap); see Fig. 7.

Among the disordered models, the critical porosity φ_c is lowest for the quantizer spheres [0.0179(8)]. For the lattices, the lowest value is attained by the BCC lattice (0.0055...). In contrast, the critical porosity of the FCC lattice [0.0358(6)] is even larger than that of overlapping spheres [0.0298(10)]. The large difference between φ_c for BCC and FCC lattices is related to the shape of the holes between the overlapping soft sphere shells. For the BCC lattice, there are only small, so-called tetrahedral holes, but for the FCC lattice, there is an additional, relatively large type of hole, called octahedral. These octahedral holes are formed by six neighboring spheres, whose centers form a regular octahedron; the interstice between the spheres has a shape that resembles a cube (which is the dual polyhedron of an octahedron); see Fig. 6.

Next, we compare the critical pore radius to the pore-size statistics. We have found the following mean pore sizes (compared at unit number density): for overlapping spheres, $\langle\delta\rangle = 0.30933...$ at $\phi_1 = 0.9148...$ and $\langle\delta\rangle = 0.14346...$ at $\phi_1 = 0.3640...$; for equilibrium hard spheres, $\langle\delta\rangle = 0.10259(2)$; for SC HS, $\langle\delta\rangle = 0.09602...$; for quantizer spheres, $\langle\delta\rangle = 0.06881(1)$ at $\phi_1 = 0.430$ and $\langle\delta\rangle = 0.05990(1)$ at $\phi_1 = 0.364$; for MRJ HS, $\langle\delta\rangle = 0.067414(8)$; for BCC HS, $\langle\delta\rangle = 0.05095...$; and for FCC HS, $\langle\delta\rangle = 0.04674...$. Table II lists the second moments of the pore sizes for our models.

Following the suggestion by Torquato [7], Fig. 8 compares the square of the critical pore radius to the second moments of the pore size. To compare the models for a broad range of porosities, we here vary the sphere radii R for each model

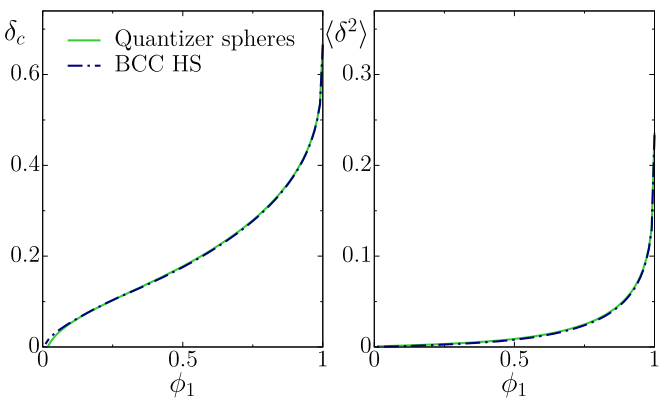

FIG. 7. The critical pore radius, δ_c (left), and the second moment of the pore size, $\langle\delta^2\rangle$ (right), are compared for dispersions of spheres arranged either on a BCC lattice or according to our amorphous inherent structures of the quantizer energy.

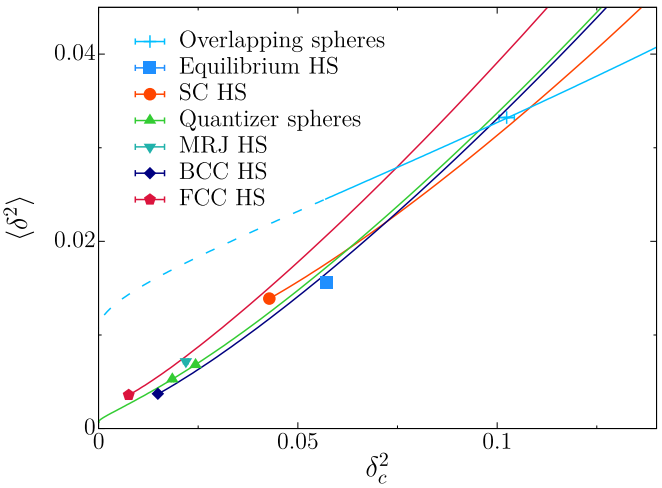

FIG. 8. Comparison of the square of the critical pore radius δ_c^2 and the second moment of the pore-size distribution δ^2: The curves represent different values of δ_{SH} with fixed sphere centers. For precise values, see Table II. The solid and dashed lines represent overlapping spheres with porosities above and below 0.23. For the entire range of our models and porosities, we find $\delta_c^2 \propto \delta^2$ to a good approximation for models with a well-connected pore space. However, as shown in Figs. 9 and 10, δ_c^2 and δ^2 predict different rankings of the fluid permeability k for dispersions of spheres at a given volume fraction.

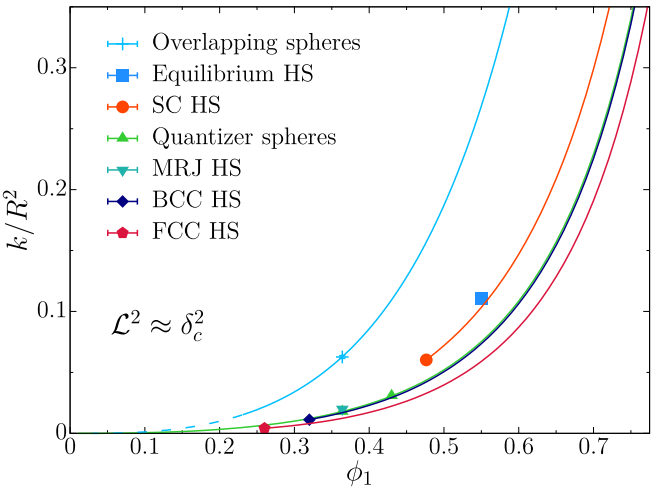

FIG. 9. Estimate of permeability as a function of porosity for our hard- and overlapping-sphere models, where $\mathcal{L}^2$ is approximated by δ_c^2.

(from 0 to ∞). In agreement with the suggestion, we find that δ_c is, to a good approximation, proportional to $\langle\delta^2\rangle$ over our entire range of models and porosities. However, δ_c^2 and δ^2 lead to different predictions of the rankings of the fluid permeability k for dispersions of spheres at a given volume fraction, as discussed below.

The approximation of $\mathcal{L}^2$ by $\langle\delta^2\rangle$ was suggested by Torquato [7] for models in which the pore space is well connected. We, therefore, distinguish between overlapping-sphere configurations above (solid line) and below (dashed line) a porosity of 0.23. The approximation is most accurate for overlapping spheres if the porosity is similar to that of MRJ spheres.

For an estimate of the fluid permeability k, we additionally need to approximate the formation factor $\mathcal{F}$. Torquato [61] derived a tight lower bound on $\mathcal{F}$ for any three-dimensional porous medium that accounts for up to four-point information. For both ordered and disordered dispersions of particles, the four-point parameter vanishes to a very good approximation, which yields the following approximation for the formation factor:

$$\mathcal{F} \approx \frac{2+\phi_2-\phi_1\zeta_2}{\phi_1(2-\zeta_2)}. \tag{5}$$

Here $\zeta_2 \in [0, 1]$ is a *three-point microstructural parameter*, which is a weighted integral involving the one-, two-, and three-point correlation functions S_1, S_2, and S_3. The high predictive power of Eq. (5) has already been validated by excellent agreement with computer simulations of $\mathcal{F}$ for a variety of ordered and disordered dispersions of spheres in a matrix [61–66]. When $\zeta_2 = 0$, Eq. (5) reduces to the well-known two-point Hashin-Shtrikman lower bound on $\mathcal{F}$ (which is optimal for given one- and two-point correlation functions S_1 and S_2) [1,67].

Here we use for our lattice sphere packings the tabulated values of ζ_2 up to the maximal packing fractions from Table 20.1 (on p. 523) in Torquato [1], which is based on data from McPhedran and Milton [68]. We interpolate the values of $\zeta_2(\phi_2)$ using fourth-order polynomials. For overlapping and equilibrium hard spheres, we use the tabulated values of ζ_2 from Table 22.1 (on p. 598) in Torquato [1], which is based on data from Torquato *et al.* [69] and Miller and Torquato [70], respectively. In these two cases of disordered spheres, an interpolation with third-order polynomials was sufficient. We use the polynomial fit to the equilibrium hard-sphere data also for an extrapolation to $\phi_2 = 0.64$, i.e., to estimate $\zeta_2 \approx 0.148$ for the MRJ sphere packings. Since no data for ζ_2 is yet available for our quantizer packings, we use the Hashin-Shtrikman lower bound in this case.

Figure 9 shows the resulting estimate of the fluid permeability k using the approximation by Katz and Thompson [10], where we choose the empirical proportionality constant between $\mathcal{L}$ and δ_c to be unity, i.e., $\mathcal{L} \approx \delta_c$. The estimate of k is highest for the uncorrelated overlapping spheres (among our models and range of porosities); in particular, k is higher for the overlapping spheres than for the hard-sphere models (both ordered and disordered), which is consistent with the theoretical predictions from Ref. [7].

Notably, the approximation by δ_c in Fig. 9 provides an inaccurate ranking of the fluid permeability of BCC and FCC sphere packings compared to theoretical calculations of the fluid permeability [71]. This inaccuracy is due to the approximation of $\mathcal{L}$ by δ_c rather than the approximation of $\mathcal{F}$, since we obtain the same ranking using the Hashin-Shtrikman and three-point approximations. In contrast, the approximation $\mathcal{L}^2 \approx \langle\delta^2\rangle$ results in the correct ranking of the fluid permeability k for FCC and BCC sphere packings, as shown in Fig. 10. Moreover, except for the quantizer model that was not studied in Ref. [7], it was shown that the approximation $\mathcal{L}^2 \approx \langle\delta^2\rangle$ provides the correct ranking for all other models

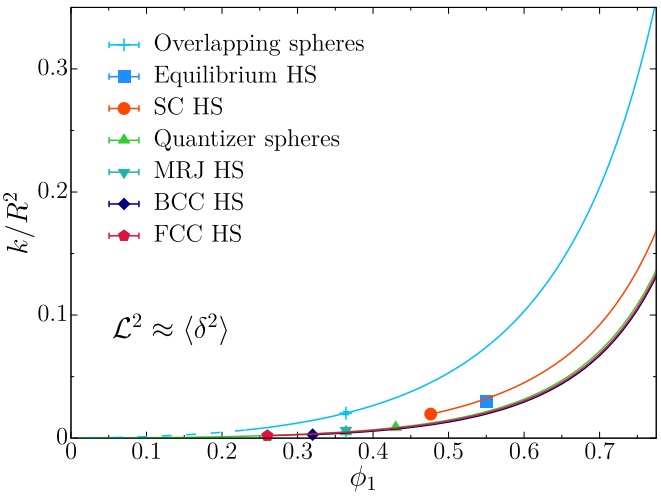

FIG. 10. Estimate of permeability as a function of porosity for our hard- and overlapping-sphere models, where $\mathcal{L}^2$ is approximated by $\langle \delta^2 \rangle$.

shown in Figs. 9 and 10. Thus, it is reasonable to expect that this approximation would properly rank the quantizer model.

IV. CONCLUSION AND OUTLOOK

We have determined the percolation threshold for void percolation around sphere configurations for models of both hard and overlapping spheres. Our examples include the MRJ packings of spheres, equilibrium fluids of hard spheres, overlapping spheres, and inherent structures of the quantizer energy, as well as ordered lattice packings of hard spheres.

To accurately determine the critical pore radius for our models, we use the strict relation to a weighted bond percolation on the Voronoi network. Moreover, we employ the Newman-Ziff algorithm and carefully take finite-system size effects into account. We compare our results in Table II to the second moment of the pore size δ.

We find in Fig. 8 a remarkably good correlation between δ_c^2 and $\langle \delta^2 \rangle$ across our broad spectrum of highly ordered and disordered sphere configurations, confirming the suggestion by Torquato [7]. Since $\langle \delta^2 \rangle$ can be easily measured from two- or three-dimensional digitized images of heterogeneous materials, this recent approximation of $\mathcal{L}^2$ by $\langle \delta^2 \rangle$ allows for a simple yet reliable prediction of the permeability k. In fact, we find that, in contrast to the critical pore size δ_c, the second moment of the pore size, $\langle \delta^2 \rangle$, predicts the correct ranking of k for our models.

Moreover, we observe that the hyperuniform and effectively hyperuniform models, like the most hyperuniform BCC sphere packing or the disordered MRJ and quantizer packings, tend to have smaller estimates of k than the nonhyperuniform overlapping or equilibrium hard spheres. This again agrees with theoretical arguments from Torquato [7] that k can be expected to be lower in hyperuniform than in nonhyperuniform porous media because the latter exhibit a greater variability in the sizes and geometries of the pore channels. Hence, the velocity fields will be generally more uniform throughout the pore space for hyperuniform two-phase media compared to their nonhyperuniform counterparts. This is also consistent with the fact that the BCC sphere packings have the lowest fluid permeabilities, since the BCC lattice is the structure with the lowest value of the hyperuniformity order metric, implying that it suppresses large-scale density fluctuations to the greatest degree [38,39]. It is interesting to point out that the BCC lattice is also the optimum of the covering and quantizer problems [34]. Our results provide additional confirmation for the analysis presented in Torquato [7] for the aforementioned link between these optimization problems, the pore statistics, and fluid permeability.

Since the empirical Katz-Thomson formula has already been applied to a broad variety of microstructures [10,12,13], a possible direction for future research is to test the approximation of δ_c^2 by $\langle \delta^2 \rangle$ for polydisperse sphere configurations and more complex particle shapes, that is, for more general models of porous media as long as the pore space remains well-connected. This condition is important for the theoretical arguments of the approximation of $\mathcal{L}^2$ by $\langle \delta^2 \rangle$.

An important outstanding problem is then to directly determine fluid permeabilities from Stokes-flow simulations (as suggested in Ref. [7]). Another direction for future research is the determination of other transport properties besides the permeability, e.g., the effective electrical or thermal conductivity of void space (possibly represented by the Voronoi network).

ACKNOWLEDGMENTS

We thank Jaeuk Kim for his samples of equilibrium hard spheres. M.A.K. and S.T. were supported in part by the Princeton University Innovation Fund for New Ideas in the Natural Sciences and by the Air Force Office of Scientific Research Program on Mechanics of Multifunctional Materials and Microsystems under Award No. FA9550-18-1-0514. M.A.K. also acknowledges funding by the Volkswagenstiftung via the Experiment-Projekt Mecke.

[1] S. Torquato, in *Random Heterogeneous Materials*, 2nd ed., edited by S. S. Antman, L. Sirovich, J. E. Marsden, and S. Wiggins, Interdisciplinary Applied Mathematics, Vol. 16 (Springer, New York, 2002).
[2] S. Prager, Chem. Eng. Sci. **18**, 227 (1963).
[3] S. Torquato and M. Avellaneda, J. Chem. Phys. **95**, 6477 (1991).
[4] We depart from the usual notation of τ for the mean survival time to avoid a conflict in notation with the τ order metric.
[5] M. Avellaneda and S. Torquato, Phys. Fluids A **3**, 2529 (1991).
[6] J. Rubinstein and S. Torquato, J. Fluid Mech. **206**, 25 (1989).
[7] S. Torquato, Adv. Water Resour. **140**, 103565 (2020).
[8] S. Torquato, Phys. Rev. Lett. **64**, 2644 (1990).
[9] A. E. Scheidegger, *The Physics of Flow Through Porous Media* (University of Toronto Press, Toronto, 1974).
[10] A. J. Katz and A. H. Thompson, Phys. Rev. B **34**, 8179 (1986).

[11] D. L. Johnson, J. Koplik, and L. M. Schwartz, Phys. Rev. Lett. **57**, 2564 (1986).
[12] N. Martys and E. J. Garboczi, Phys. Rev. B **46**, 6080 (1992).
[13] N. Nishiyama and T. Yokoyama, J. Geophys. Res. Solid Earth **122**, 6955 (2017).
[14] J. L. Finney, Nature (London) **266**, 309 (1977).
[15] R. Zallen, *The Physics of Amorphous Solids* (Wiley, New York, 1998).
[16] P. M. Chaikin and T. C. Lubensky, *Principles of Condensed Matter Physics* (Cambridge University Press, Cambridge, 2000).
[17] V. N. Manoharan, M. T. Elsesser, and D. J. Pine, Science **301**, 483 (2003).
[18] J.-P. Hansen and I. R. McDonald, *Theory of Simple Liquids: With Applications to Soft Matter*, 4th ed. (Academic Press, Amsterdam, 2013).
[19] S. Torquato, T. M. Truskett, and P. G. Debenedetti, Phys. Rev. Lett. **84**, 2064 (2000).
[20] S. Torquato and F. H. Stillinger, Rev. Mod. Phys. **82**, 2633 (2010).
[21] C. S. O'Hern, S. A. Langer, A. J. Liu, and S. R. Nagel, Phys. Rev. Lett. **88**, 075507 (2002).
[22] N. C. Karayiannis and M. Laso, Phys. Rev. Lett. **100**, 050602 (2008).
[23] X. Xu and S. A. Rice, Phys. Rev. E **83**, 021120 (2011).
[24] M. Ozawa, T. Kuroiwa, A. Ikeda, and K. Miyazaki, Phys. Rev. Lett. **109**, 205701 (2012).
[25] V. Baranau, D. Hlushkou, S. Khirevich, and U. Tallarek, Soft Matter **9**, 3361 (2013).
[26] J. Tian, Y. Xu, Y. Jiao, and S. Torquato, Sci. Rep. **5**, 16722 (2015).
[27] Y. Jiao, F. H. Stillinger, and S. Torquato, J. Appl. Phys. **109**, 013508 (2011).
[28] S. Atkinson, F. H. Stillinger, and S. Torquato, Phys. Rev. E **88**, 062208 (2013).
[29] M. A. Klatt and S. Torquato, Phys. Rev. E **90**, 052120 (2014).
[30] M. A. Klatt and S. Torquato, Phys. Rev. E **94**, 022152 (2016).
[31] M. A. Klatt and S. Torquato, Phys. Rev. E **97**, 012118 (2018).
[32] R. M. Ziff and S. Torquato, J. Phys. A: Math. Theor. **50**, 085001 (2017).
[33] M. A. Klatt, J. Lovrić, D. Chen, S. C. Kapfer, F. M. Schaller, P. W. A. Schönhöfer, B. S. Gardiner, A.-S. Smith, G. E. Schröder-Turk, and S. Torquato, Nature Commun. **10**, 811 (2019).
[34] S. Torquato, Phys. Rev. E **82**, 056109 (2010).
[35] S. Torquato, G. Zhang, and F. H. Stillinger, Phys. Rev. X **5**, 021020 (2015).
[36] A. R. Kerstein, J. Phys. A: Math. Gen. **16**, 3071 (1983).
[37] M. E. J. Newman and R. M. Ziff, Phys. Rev. E **64**, 016706 (2001).
[38] S. Torquato and F. H. Stillinger, Phys. Rev. E **68**, 041113 (2003).
[39] S. Torquato, Phys. Rep. **745**, 1 (2018).
[40] C. E. Zachary and S. Torquato, J. Stat. Mech. (2009) P12015.
[41] Y. Liu, W. Wang, B. Lévy, F. Sun, D.-M. Yan, L. Lu, and C. Yang, ACM Trans. Graph. **28**, 1 (2009).
[42] Q. Du, M. Gunzburger, and L. Ju, Numer. Math. Theor. Meth. Appl. **3**, 119 (2010).
[43] J. Zhang, M. Emelianenko, and Q. Du, Int. J. Numer. Anal. Model. **9**, 950 (2012).
[44] C. Ruscher, J. Baschnagel, and J. Farago, Europhys. Lett. **112**, 66003 (2015).
[45] C. Ruscher, J. Baschnagel, and J. Farago, Phys. Rev. E **97**, 032132 (2018).
[46] C. Ruscher, S. Ciarella, C. Luo, L. M. C. Janssen, J. Farago, and J. Baschnagel, J. Phys.: Condens. Matter **33**, 064001 (2020).
[47] T. M. Hain, M. A. Klatt, and G. E. Schröder-Turk, J. Chem. Phys. **153**, 234505 (2020).
[48] M. D. Rintoul, Phys. Rev. E **62**, 68 (2000).
[49] S. Lloyd, IEEE Trans. Inf. Theory **28**, 129 (1982).
[50] W. T. Elam, A. R. Kerstein, and J. J. Rehr, Phys. Rev. Lett. **52**, 1516 (1984).
[51] F. Höfling, T. Munk, E. Frey, and T. Franosch, J. Chem. Phys. **128**, 164517 (2008).
[52] D. J. Priour and N. J. McGuigan, Phys. Rev. Lett. **121**, 225701 (2018).
[53] M. Spanner, F. Höfling, S. C. Kapfer, K. R. Mecke, G. E. Schröder-Turk, and T. Franosch, Phys. Rev. Lett. **116**, 060601 (2016).
[54] J. D. Treado, Z. Mei, L. Regan, and C. S. O'Hern, Phys. Rev. E **99**, 022416 (2019).
[55] C. H. Rycroft, G. S. Grest, J. W. Landry, and M. Z. Bazant, Phys. Rev. E **74**, 021306 (2006).
[56] C. H. Rycroft, Chaos **19**, 041111 (2009).
[57] J. Wang, Z. Zhou, W. Zhang, T. M. Garoni, and Y. Deng, Phys. Rev. E **87**, 052107 (2013).
[58] D. Coker, S. Torquato, and J. Dunsmuir, J. Geophys. Res. B Solid Earth **101**, 17497 (1996).
[59] Note the different scaling of the first and second moment of the pore size in Ref. [31]. There, the values are given for unit diameter of the spheres; here, we list the values for unit number density.
[60] For the overlapping sphere model (also known as Boolean model), where the sphere centers are uncorrelated, R_c is strictly related to the critical porosity of the percolating void phase, $\phi_c = \exp[-\rho v_1(R_c)]$, where $v_1(R_c)$ is the volume of a ball with radius R_c [1].
[61] S. Torquato, J. Appl. Phys. **58**, 3790 (1985).
[62] I. C. Kim and S. Torquato, J. Appl. Phys. **69**, 2280 (1991).
[63] D. A. Robinson and S. P. Friedman, Physica A **358**, 447 (2005).
[64] A. Gillman and K. Matouš, Phys. Lett. A **378**, 3070 (2014).
[65] A. Gillman, G. Amadio, K. Matouš, and T. L. Jackson, Proc. R. Soc. A **471**, 20150060 (2015).
[66] M.-T. Nguyen, V. Monchiet, G. Bonnet, and Q.-D. To, Phys. Rev. E **93**, 022105 (2016).
[67] Z. Hashin and S. Shtrikman, J. Mech. Phys. Solids **11**, 127 (1963).
[68] R. C. McPhedran and G. W. Milton, Appl. Phys. A **26**, 207 (1981).
[69] S. Torquato, G. Stell, and J. Beasley, Int. J. Eng. Sci. **23**, 385 (1985).
[70] C. A. Miller and S. Torquato, J. Appl. Phys. **68**, 5486 (1990).
[71] A. Sangani and A. Acrivos, Int. J. Multiphase Flow **8**, 343 (1982).